Modeling Electroporation in a Single Cell. II. Effects of Ionic Concentrations

Katherine A. DeBruin, Ph.D. and Wanda Krassowska, Ph.D.
Department of Biomedical Engineering and Center for Emerging Cardiovascular Technologies, Duke University, Durham, North Carolina, USA

ABSTRACT This study expands a previously developed model of a single cell electroporated by an external electric field by explicitly accounting for the ionic composition of the electroporation current. The previous model with non-specific electroporation current predicts that both the transmembrane potential V_m and the pore density N are symmetric about the equator, with the same values at either end of the cell. The new, ion-specific case predicts that V_m is symmetric and almost identical to the profile from the non-specific case, but N has a profound asymmetry with the pore density at the hyperpolarized end of the cell twice the value at the depolarized end. These modeling results agree with the experimentally observed preferential uptake of marker molecules at the hyperpolarized end of the cell as reported in the literature. This study also investigates the changes in intracellular ionic concentrations induced around an electroporated single cell. For all ion species, the concentrations near the membrane vary significantly, which may explain the electrical disturbances observed experimentally after large electric shocks are delivered to excitable cells and tissues.

INTRODUCTION

Electroporation is a protective feature common to all lipid bilayers in which conductive pores form in the membrane when the transmembrane potential V_m exceeds a critical value. These pores shunt the excess stimulus current across the membrane, limiting the growth of the transmembrane potential and preventing permanent damage to the membrane. Once formed, the pores often survive in the membrane for seconds to minutes, providing pathways for the exchange of water, ions, and macromolecules between intracellular and extracellular space. This feature has made electroporation a common tool in biotechnology (Chang et al., 1992; Neumann et al., 1989), and many researchers are studying both the beneficial and detrimental effects of electroporation in medical applications (River et al., 1991; Tsong, 1991; Tung et al., 1995; Zhang et al., 1996).

Until recently, theoretical models of electroporation were too complex and computationally time consuming to be applied to spatially extended tissues such as single cells, fibers, and two-dimensional sheets. With the development of the macroscopic model of electroporation (DeBruin and Krassowska, 1998, 1999; Krassowska, 1995; Neu and Krassowska, 1999), it is now possible to study both the temporal and spatial variation of electroporation along with its interaction with the transmembrane potential. In Part I of this study (DeBruin and Krassowska, 1999), a model of an electroporating single cell was developed and used to investigate the effects of shock strength and rest potential on the transmembrane potential V_m and pore density N around the cell. The model confirmed the experimental observation that electroporation lowers V_m as compared to the potential induced in a cell with a resistive-capacitive membrane, with the largest decrease occurring at the poles of the cell and the smallest near the equator. The expected cosinusoidal shape of the V_m profile is flattened near the poles of an electroporated cell, because the pore density N increases with induced potential such that V_m remains nearly constant throughout the electroporated region.

The majority of the modeling results reported in Part I of this study qualitatively and quantitatively matched the experimental data reported by Kinosita and coworkers for unfertilized sea urchin eggs (Hibino et al., 1991, 1993; Kinosita et al., 1988, 1991, 1992). The only significant discrepancy between the modeling and experimental results concerns the symmetry or asymmetry of the electroporation process. The model predicts that both the pore density N and the transmembrane potential V_m are symmetric about the equator: the value of N is the same at the depolarized and hyperpolarized ends of the cell, and V_m differs only in polarity. Experimentally, only one study reports a possible asymmetry in transmembrane potential during the first microsecond of the shock (Hibino et al., 1993), but almost all investigations show an asymmetric uptake of marker molecules by an electroporated cell (Djuzenova et al., 1996; Gabriel and Teissie, 1997; Knisley and Grant, 1995; Mehrle et al., 1985, 1989; Rossignol et al., 1983; Tekle et al., 1990; Teruel and Meyer, 1997). Regardless of the cell type, the size or charge of the marker molecule, or the shock protocol, these researchers observed preferential molecular uptake at the hyperpolarized end of the cell. Many of the studies attribute this asymmetry to the rest potential V_{rest} (Djuzenova et al., 1996); (Gabriel and Teissie, 1997); (Mehrle et al., 1985); (Mehrle et al., 1989); (Tekle et al., 1990), as its negative value is thought to bias electroporation toward the hyperpolarized pole. However, two experi-

Received for publication 23 December 1998 and in final form 3 June 1999.
Address reprint requests to Katherine A. DeBruin, Ph.D., Department of Biomedical Engineering, Box 90281, Duke University, Durham, North Carolina 27708-0281. Tel.: 919-660-5131; Fax: 919-684-4488; E-mail: kad3@eel-mail.mc.duke.edu.

0006-3495/99/09/1225/09 $2.00

mental studies tested cells in bathing solutions that eliminated V_{rest}, and the preferential uptake of marker molecules at the hyperpolarized end of the cell was still observed (Knisley and Grant, 1995; Teruel and Meyer, 1997). The model of electroporation presented in Part I confirmed that altering V_{rest} would produce only a very minor asymmetry in N, not enough to explain the experimentally observed results (DeBruin and Krassowska, 1999).

Therefore, the true cause of the experimentally observed asymmetry in the uptake of marker molecules during electroporation must be due to other factors, such as an inherent asymmetry in the lipid bilayer (Genco et al., 1993) or an interaction between the pores and other membrane structures. This study explores a third possibility that the asymmetry is due to ionic concentration gradients across the membrane. To investigate this hypothesis, the model of electroporation has been expanded to account explicitly for the ionic composition of the electroporation current and to include the contributions of an arbitrary number of ion species. This new, ion-specific model will be used to address two questions: 1) do ionic concentrations influence the creation of pores during the shock, and 2) to what extent does the presence of pores change the intracellular ionic concentrations. The modeling results will be compared to experimental data reported in the literature (Djuzenova et al., 1996; Gabriel and Teissie, 1997; Hibino et al., 1993; Knisley and Grant, 1995; Mehrle et al., 1985, 1989; Rossignol et al., 1983; Tekle et al., 1990; Teruel and Meyer, 1997).

METHODS

Representation of an electroporating cell

A spherical single cell immersed in an extracellular bath is treated as a source-free system in which the intracellular and extracellular potentials Φ_i and Φ_e obey Laplace's equation. The electric field is applied as a boundary condition on the outer edge of the extracellular space. In the membrane, the intracellular and extracellular current are both equal to the transmembrane current I_m,

$$I_m = C_m \frac{\partial V_m}{\partial t} + I_{ion} + I_{ep}, \tag{1}$$

where C_m is the specific membrane conductance and $V_m \equiv \Phi_i - \Phi_e$ is the transmembrane potential. I_{ion} is the ionic current, here assumed to be passive and equal to $g_l(V_m - E_l)$, where g_l is the leakage conductance of the membrane and E_l is the reversal potential. I_{ep} is the electroporation current due to the movement of ions through the shock-induced pores,

$$I_{ep} = N i_{ep}, \tag{2}$$

where N is the pore density and i_{ep} is the current through a single pore. The pore density N is governed by a first-order differential equation (DeBruin and Krassowska, 1998, 1999; Neu and Krassowska, 1999),

$$\frac{dN}{dt} = \alpha e^{(V_m/V_{ep})^2}\left(1 - \frac{N}{N_o} e^{-q(V_m/V_{ep})^2}\right), \tag{3}$$

where N_o is the pore density when $V_m = 0$ mV, and α, V_{ep}, and q are experimentally determined constants.

As an example, this study will use the same spherical single cell considered in Part I with the same parameters. The cell parameters (diameter, passive kinetics), stimulus protocol (electric field strength, duration), material constants (intracellular, extracellular conductivities), and electroporation characteristics (significant effects at $V_m \approx 1$ V) are matched to the values reported by Kinosita and coworkers for unfertilized sea urchin eggs (Hibino et al., 1991, 1993; Kinosita et al., 1988, 1991, 1992). For a rest potential of −80 mV (Chambers and Armendi, 1979), the reversal potential of the ionic current E_l is set to −83.75 mV. The shock protocol consists of a 400-V/cm field applied for a duration of 1 ms. The electroporation parameters α and N_o are based on experimental results from artificial lipid bilayers (Glaser et al., 1988), whereas V_{ep} was chosen such that electroporation becomes significant at a critical transmembrane potential V_{cr} of approximately 1 V. Values for all parameters are the same as in Part I of this study and are given in Table 1 of Part I (DeBruin and Krassowska, 1999). The system of equations was solved using a combined finite difference/singular perturbation method that is described in detail in Part I of this study (DeBruin and Krassowska, 1999). All simulations were performed on a Sun Ultra 1 workstation.

Ion-specific electroporation current

In this study, the current through a single pore i_{ep} is comprised of four ion species, Na^+, K^+, Ca^{2+}, and Cl^-, which are the ions typically present in an excitable cell (DiFrancesco and Noble, 1985; Luo and Rudy, 1994). The derivation of the expression for i_{ep} is based on the method used by Barnett, in which only two monovalent, oppositely charged ion species were present with the same concentrations on both sides of the membrane (Barnett, 1990). These restrictions on the ion species were discarded for this study, and a complete derivation of i_{ep} is given in the Appendix. For an arbitrary number of ion species x, i_{ep} is computed from the formula,

$$i_{ep} = \frac{\pi r_m^2 F v_m}{h} \sum_x \frac{D_x z_x^2([x]_i \exp(z_x v_m) - [x]_o)}{\mathcal{A} \exp(z_x v_m) - \mathcal{B}}, \tag{4}$$

where

$$\mathcal{A} = \frac{w_o z_x \exp[z_x(w_o z_x - n v_m)] - n v_m}{w_o z_x - n v_m},$$

$$\mathcal{B} = \frac{w_o z_x \exp[z_x(w_o z_x + n v_m)] + n v_m}{w_o z_x + n v_m}$$

where r_m is the radius of the pore, F is Faraday's constant, h is the thickness of the membrane, D_x is the diffusion coefficient and z_x is the valence of ion species x, $[x]_i$ and $[x]_o$ are the intracellular and extracellular concentrations, and n is the relative entrance length of the pore. On the right-hand side, v_m is the nondimensional transmembrane potential, $v_m \equiv V_m(F/RT)$ where R is the universal gas constant and T is the absolute temperature. The same energy barrier w_o is assumed for all ion species.

The ion-specific electroporation current i_{ep} has a non-zero reversal potential E_{rev} which can be computed using a form of Goldman's equation that incorporates both monovalent and divalent ions (Jan and Jan, 1976),

$$E_{rev} = \frac{RT}{F} \ln\left(\frac{-b + \sqrt{b^2 - 4ac}}{2a}\right), \tag{5}$$

where

$$a = [K^+]_i + \frac{p_{Cl}}{p_K}[Cl^-]_o + 4\frac{p_{Ca}}{p_K}[Ca^{2+}]_i + \frac{p_{Na}}{p_K}[Na^+]_i,$$

$$b = ([K^+]_i - [K^+]_o) - \frac{p_{Cl}}{p_K}([Cl^-]_i - [Cl^-]_o) + \frac{p_{Na}}{p_K}([Na^+]_i - [Na^+]_o),$$

$$c = -[K^+]_o - \frac{p_{Cl}}{p_K}[Cl^-]_i - 4\frac{p_{Ca}}{p_K}[Ca^{2+}]_o - \frac{p_{Na}}{p_K}[Na^+]_o .$$

p_x is the permeability of ion species x, defined as $p_x = D_x\beta_x/h$, where β_x is the partition coefficient of ion species x (Plonsey and Barr, 1988). This study assumes that β_x is the same for all ions, so the permeabilities in Eq. 5 can be replaced by the diffusion coefficients D_x. For the four ion species used in this study, with the concentrations and diffusion coefficients listed in Table 1, $E_{rev} = -21.8$ mV. This value is similar to the reversal potential of approximately -35 mV estimated by Neunlist and Tung (1997) for electroporated frog ventricular cells. In comparison, the non-specific electroporation current used in Part I of this study had a reversal potential of 0 mV (DeBruin and Krassowska, 1999).

Intracellular concentrations

One goal of this study is to investigate the changes in the intracellular ionic concentrations caused by the electroporation current. At any location within the cell, the rate of change of the intracellular ionic concentration $[x]_i$ can be described by a partial differential equation,

$$\frac{\partial [x]_i}{\partial t} = \nabla \cdot \left(D_x \nabla [x]_i + \frac{D_x z_x F}{RT}[x]_i \nabla \Phi_i \right), \qquad (6)$$

where t is time and Φ_i is the intracellular potential. On the right-hand side, the first term describes the movement of ions due to diffusion, and the second term is the drift of ions in the intracellular electric field induced by the polarization of the cell. For the spherical cell considered in this study, Eq. 6 can be simplified. For diffusion, the characteristic length scale is $\delta_x = \sqrt{6D_x t}$ (Hille, 1992), and, during a 1-ms shock, the ions will diffuse an average of 2.2–3.5 μm from the membrane toward the center of the cell. For drift, the distance traveled is $D_x z_x t(F/RT)\nabla\Phi_i$. With a 400-V/cm, 1-ms pulse, $|\nabla\Phi_i|$, in an electroporated cell, is 363 V/cm, and the ions move 1.9–2.9 μm. The estimates of the characteristic length for both diffusion and drift amount to less than 7% of the cell's radius $a = 50$ μm.

Based on the above estimates, this study modeled only local changes in the intracellular concentrations. Assuming that 1) concentrations change only in a layer of thickness δ_x adjacent to the membrane, 2) the exchange of ions between this layer and the rest of the cell can be neglected, and 3) the movement of ions within this layer can also be neglected, $[x]_i$ depends only on the influx or efflux of ions x through the pores at each point around the cell. The rate of change of $[x]_i$ is governed by an ordinary differential equation,

$$\frac{d[x]_i}{dt} = -\frac{1}{\delta_x}\frac{N i_{ep,x}}{z_x F}, \qquad (7)$$

where $i_{ep,x}$ is the electroporation current carried by ion species x. For this study, the values of δ_x were chosen to be the characteristic length scale for diffusion of each ion species and are listed in Table 1. For simplicity, the extracellular ionic concentrations were kept constant.

TABLE 1 Ion species parameters

Ion	$[x]_i$ (mM)	$[x]_o$ (mM)	D_x (cm^2/s)	δ_x (cm)
Na^+	22.0	151.0	1.33×10^{-5}	2.8×10^{-4}
K^+	145.0	4.5	1.96×10^{-5}	3.4×10^{-4}
Ca^{2+}	0.00017	1.8	0.79×10^{-5}	2.2×10^{-4}
Cl^-	4.0	103.0	2.04×10^{-5}	3.5×10^{-4}

RESULTS

Effects of ionic concentrations on electroporation

Part I of this study (DeBruin and Krassowska, 1999) used the model of non-specific electroporation current to investigate the time course of the transmembrane potential V_m and the pore density N around an electroporating single cell. The results predicted by the model of ion-specific electroporation current are similar, with three notable exceptions. First, the V_m profile around the cell has a small negative offset as compared to the transmembrane potential predicted by the non-specific model (Fig. 1 *A*). The magnitude of this offset depends on position. Near the equator, $V_m \approx 0$ mV for the non-specific case and $V_m \approx -21.8$ mV for the ion-specific case, values that correspond to the reversal potentials of each model (Fig. 2 *B*). Near the poles, the magnitude of the offset decreases to less than 10 mV.

Second, the two current models predict different values of the transmembrane potential assumed by the cell immediately after the postshock discharge. Both cases find that V_m is equal to the reversal potential of the electroporation

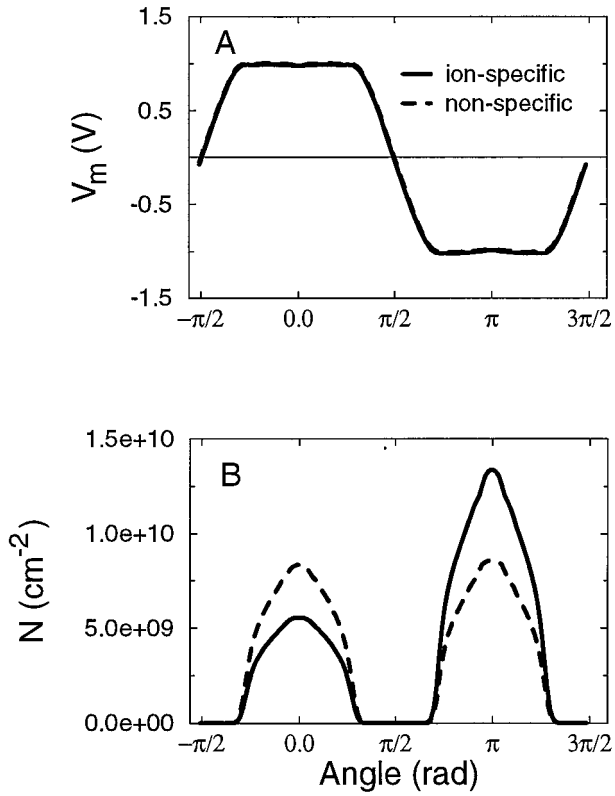

FIGURE 1 (*A*) Transmembrane potential and (*B*) pore density around a spherical cell at the end of 400-V/cm, 1-ms shock as predicted by models with non-specific (*dashed line*) and ion-specific (*solid line*) electroporation currents. V_m is almost identical for the two models, but the pore density profiles have significantly different shapes (symmetric for the non-specific case, asymmetric for the ion-specific case).

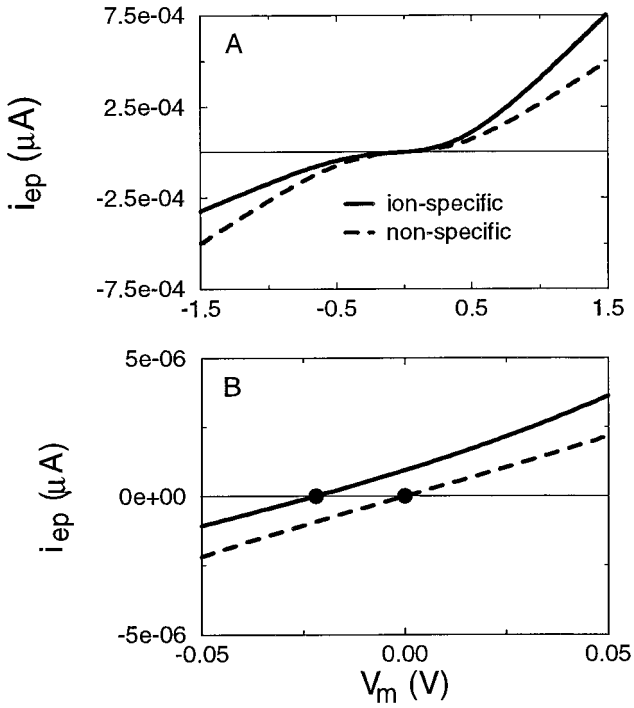

FIGURE 2 The current–voltage relationships for the non-specific (*dashed line*) and ion-specific (*solid line*) electroporation currents. (*A*) Full range of V_m used in this study. (*B*) Details of the curves for small V_m, with dots indicating reversal potentials of 0 mV for the non-specific case and −21.8 mV for the ion-specific case.

current, but that value is different for each model. The third difference between the results of the models with non-specific and ion-specific electroporation current concerns the shape of the pore density profile. The non-specific case predicts a symmetric profile in which the magnitude of N is the same at both poles, but the ion-specific case predicts a striking asymmetry in which N at the hyperpolarized pole of the cell is twice the magnitude of N at the depolarized pole (Fig. 1 *B*).

This difference in the pore density profile can be explained by considering that the net transmembrane current I_m must be zero in a source-free system like an isolated single cell. After the initial capacitive transient, the electroporation current I_{ep} is approximately four orders of magnitude larger than the ionic current I_{ion}, so $I_m \approx I_{ep} = Ni_{ep}$. With the concentrations given in Table 1, the ion-specific current is outwardly rectifying (Fig. 2 *A*). To keep I_m balanced, the larger i_{ep} at the depolarized end of the cell must be accompanied by a smaller value of N, producing the asymmetric pore density distribution seen in Fig. 1 *B*. In contrast, the non-specific case has a symmetric current–voltage relationship (Fig. 2 *A*), and the magnitude of i_{ep} is unaffected by the sign of the transmembrane potential. Consequently, the pore density distribution is symmetric (Fig. 1 *B*).

For the ion-specific case, the shape of the current–voltage curve is uniquely determined by the choice of ion species and concentrations. Different choices would lead to electroporation currents with different rectifying properties and thus to different pore density profiles. For example, if only sodium ions were present, i_{ep} would be an inwardly rectifying current with a reversal potential of approximately +45 mV, and N would be greater at the depolarized end of the cell. However, the V_m profile would remain essentially unaltered, with only a small positive offset due to the non-zero reversal potential of i_{ep} (compare to Fig. 1 *A*).

This relationship between the ionic concentration gradient and the pore density can be exploited to create a customized distribution of N around the cell. The effects of varying the extracellular concentration $[x]_o$ of each ion species x are shown in Fig. 3. For each species, altering $[x]_o$ influences N on only one end of the cell: hyperpolarized for positive ions (Na^+, K^+, Ca^{2+}) and depolarized for negative ions (Cl^-). This behavior can be explained by examining the component of the ion-specific electroporation current (Eq. 4) that involves ionic concentrations,

$$i_{ep,x} \propto [x]_i e^{z_x v_m} - [x]_o, \tag{8}$$

where $[x]_i$ and $[x]_o$ are the intracellular and extracellular concentrations and z_x is the valence of ion species x, and v_m is the nondimensional transmembrane potential. Using sodium as an example, the exponent ($z_{Na}v_m$) is negative at the hyperpolarized end of the cell. The $[Na^+]_i e^{z_{Na}v_m}$ term is very small compared to $[Na^+]_o$, and $i_{ep,Na}$ is proportional to the extracellular sodium concentration. If $[Na^+]_o$ decreases, then $i_{ep,Na}$ decreases and N must increase at the hyperpolarized end of the cell to maintain a zero net transmembrane current (Fig. 3 *A*). In contrast, at the depolarized end of the cell, the exponent ($z_{Na}v_m$) is positive, the $[Na^+]_i e^{z_{Na}v_m}$ term dominates, and the effect of $[Na^+]_o$ on $i_{ep,Na}$ is not significant.

If the goal is to increase the asymmetry of N, the best approach is to decrease the extracellular sodium concentration. With a nearly Na^+-free solution, the hyperpolarized end of the cell has a pore density approximately 25 times larger than N at the depolarized end (Fig. 3 *A*). Increasing $[Na^+]_o$ will make the pore density distribution more symmetric. Although changing the extracellular concentrations of potassium and calcium will also alter the asymmetry of N, the results are less dramatic because $[K^+]_o$ and $[Ca^{2+}]_o$ are initially small (Fig. 3, *B* and *C*). $[Cl^-]$ alters the pore density on the depolarized end, increasing the asymmetry of N with increasing extracellular concentration (Fig. 3 *D*).

Effects of electroporation current on ionic concentrations

For the simulations in this section, the intracellular ionic concentrations were allowed to change in the manner described in Methods. The cell was exposed to a 400-V/cm, 1-ms pulse, and the ions carried by the electroporation current locally altered the intracellular ionic concentrations around the cell (Fig. 4). All four ion species experienced a significant increase in concentration at one end of the cell

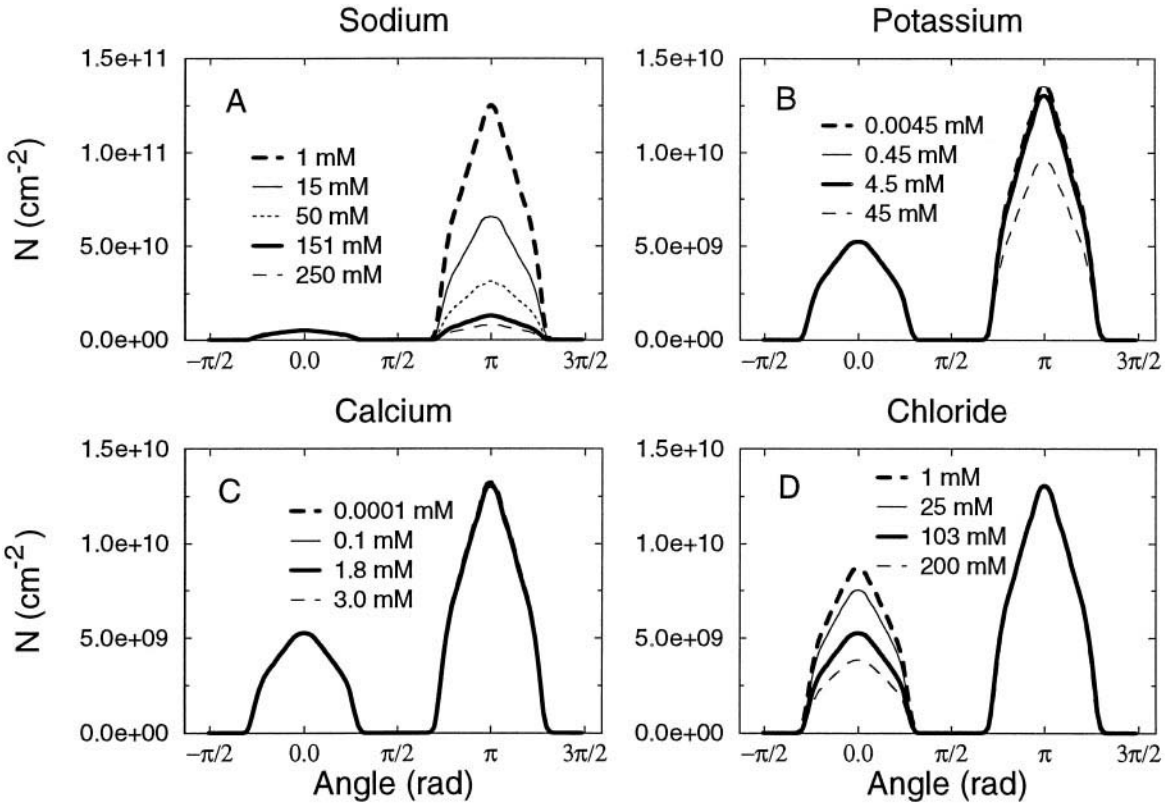

FIGURE 3 Distribution of pore density around the cell at the end of a 400-V/cm, 1-ms shock for various extracellular ionic concentrations. The heavy solid line in each panel indicates the pore density distributions for the default extracellular concentrations reported in Table 1. (*A*) Sodium, (*B*) Potassium, (*C*) Calcium, (*D*) Chloride.

and a decrease at the opposite end. Calcium exhibited the largest change, with $[Ca^{2+}]_i$ increasing by more than three orders of magnitude at the hyperpolarized end of the cell. These asymmetric changes can be explained by considering that the expression for the ion-specific electroporation current (Eq. 4) was derived from the Nernst–Planck equation (Eq. 9), in which the current due to ion species x is influenced by both the concentration and the potential gradients across the membrane. For a given positive ion species, the concentration gradient points either inward or outward, independent of position around the cell. In contrast, the potential gradient points inward at the hyperpolarized end of the cell and outward at the depolarized end. Therefore, at one end of the cell, both the concentration and potential gradients point in the same direction (inward or outward) and cause a large change in the intracellular concentration. At the other end, the gradients point in opposite directions and their effects partially cancel, but the net ion movement is always in the direction of the electrical gradient (Fig. 4).

For example, $[Na^+]_o > [Na^+]_i$, and the current due to the concentration gradient is inward. At the hyperpolarized end of the cell, the current due to the potential gradient is also inward, so both currents drive up the intracellular sodium concentration for a 471% increase at the pole. At the depolarized end, the current due to the potential gradient is outward. The two currents flow in opposite directions, but the outward current is stronger, and there is a 21% decrease in $[Na^+]_i$ at the depolarized pole of the cell. As shown in Fig. 4, the other ion species follow similar trends.

Surprisingly, these significant changes in ionic concentrations have very little effect on the distributions of V_m and N around the cell (Fig. 5). The one rather minor exception is that the transmembrane potential at the end of a 1-ms shock no longer exhibits a concavity at the depolarized pole (Fig. 5 *A*). This change can be attributed to the substantial decrease in $[K^+]_i$ at that location (Fig. 4 *B*), which decreases the potassium component of i_{ep} and forces N to increase by about 7% to keep the transmembrane current in balance (Fig. 5 *B*). A new equilibrium is established between N and V_m, producing a transmembrane potential profile without the characteristic concavity at the depolarized pole. Shock-induced changes in the intracellular concentrations of other ion species did not significantly alter either V_m or N.

DISCUSSION

Comparison to experimental results

The model of electroporation with ion-specific current predicts that the transmembrane potential profile around a single cell is symmetric, whereas the underlying pore density distribution can be significantly asymmetric. For the

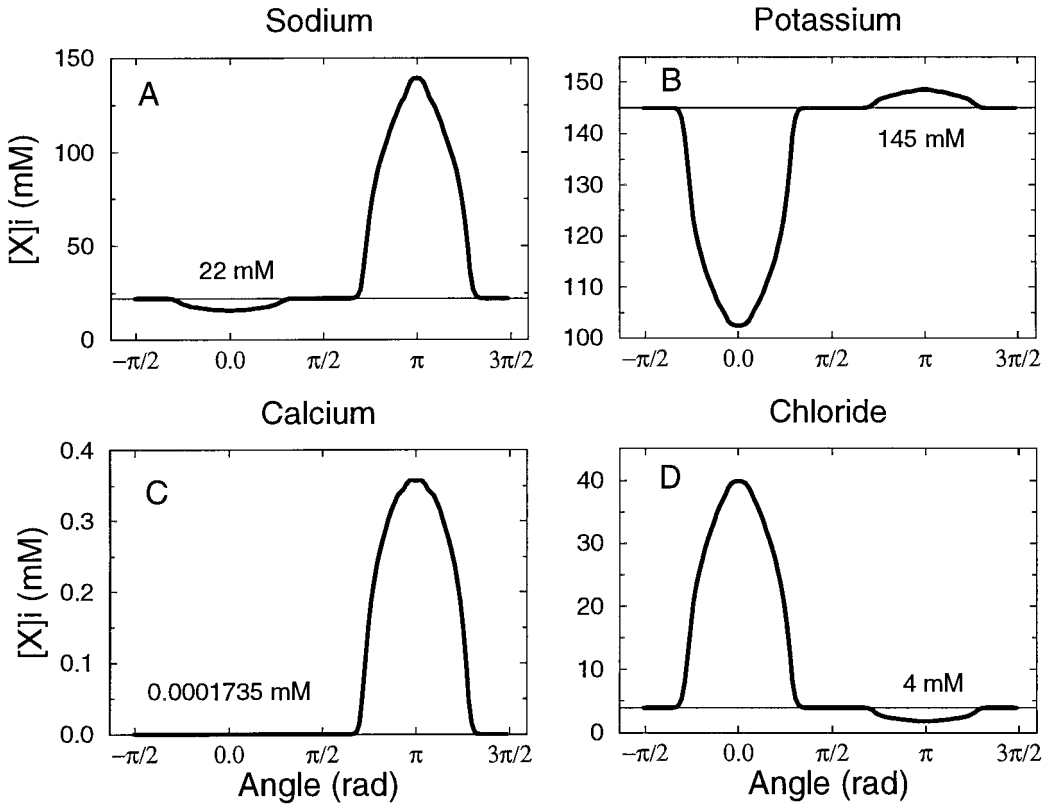

FIGURE 4 Intracellular ionic concentrations around the cell at the end of a 400-V/cm, 1-ms shock. The thin horizontal line in each panel indicates the initial intracellular concentration and is labeled with the appropriate value from Table 1. (*A*) Sodium, (*B*) Potassium, (*C*) Calcium, (*D*) Chloride.

cell used in this study, N at the hyperpolarized pole is twice the value of N at the depolarized pole. The symmetry of V_m, along with its other properties, including magnitude, time course, profile shape, and presence of concavities at the poles, agree qualitatively and quantitatively with the results from the model of electroporation with non-specific current presented in Part I of this study (DeBruin and Krassowska, 1999) and with the experimental data reported by Kinosita and coworkers for unfertilized sea urchin eggs (Hibino et al., 1991, 1993; Kinosita et al., 1988, 1991, 1992).

Given that a symmetric V_m profile does not necessarily imply that N is also symmetric, V_m alone cannot be used as an indicator of the degree of electroporation. Information on the pore density distribution must be extracted from indirect evidence concerning the movement of marker molecules into the cell. Such measurements are not specific indicators of N either, because the transport of molecules requires at least three separate conditions. First, pores must be created to provide pathways for the passage of the marker molecules across the membrane. Second, those molecules must be present in sufficient quantities near the pores, and third, some mechanism must exist to transport the molecules through the pores. Absence of marker molecules from the intracellular space may be the result of a failure in any one of these three conditions. The model of electroporation with ion-specific current does not fully describe this situation at present, so this study will assume that the location of the marker molecules is indicative of the pore density distribution, and vice versa.

The model of electroporation with ion-specific current predicts a significantly larger pore density at the hyperpolarized end of the cell (Fig. 1 *A*), implying that more molecules can be expected to cross the membrane in that region. Experimental studies (Djuzenova et al., 1996; Gabriel and Teissie, 1997; Knisley and Grant, 1995; Mehrle et al., 1985, 1989; Rossignol et al., 1983; Tekle et al., 1990; Teruel and Meyer, 1997) on a wide variety of cell types showed preferential uptake of marker molecules at the hyperpolarized end of the cell. With the exception of one study in which a neutral dye was used (Mehrle et al., 1989), all the studies used positively-charged marker molecules. The experimental measurements were taken up to several seconds after the shock, so it is not possible to determine the dominant mode of molecular transport through the pores. However, both electrophoresis of positively-charged molecules (Fig. 4) and electro-osmosis (Sowers, 1988) are consistent with influx at the hyperpolarized end of the cell. These processes will occur only during the shock, but they can significantly enhance the uptake of marker molecules beyond what may be expected from simple diffusion.

Several of these experimental studies attributed the observed asymmetric uptake of marker molecules to the intrinsic rest potential V_{rest} of the cell (Djuzenova et al., 1996; Gabriel and Teissie, 1997; Mehrle et al., 1985, 1989; Ros-

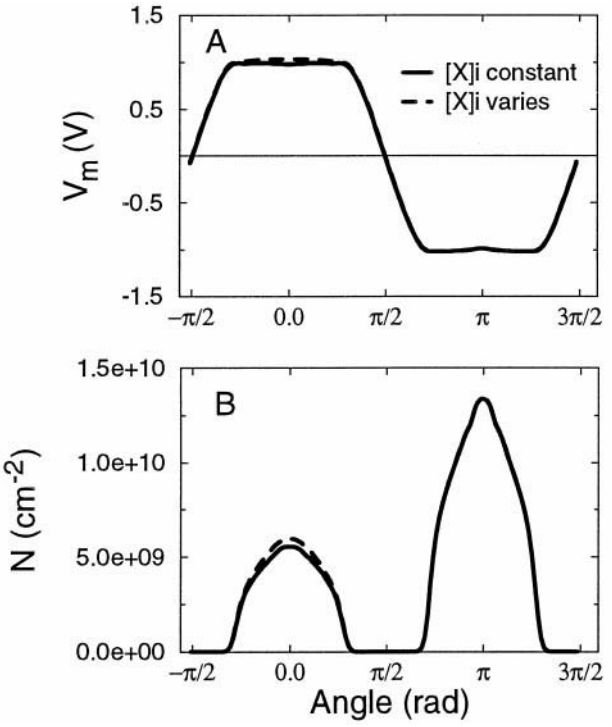

FIGURE 5 (*A*) Transmembrane potential and (*B*) pore density around a spherical cell at the end of a 400-V/cm, 1-ms shock. The solid lines indicate the results when the intracellular concentrations were held constant, and the dashed lines show the results when the intracellular concentrations were allowed to vary in time and space.

signol et al., 1983; Tekle et al., 1990). The negative value of V_{rest} was thought to bias electroporation toward the hyperpolarized end of the cell, because a smaller induced potential would be required to reach the critical value for electroporation. Two experimental studies have discredited the V_{rest} hypothesis by performing the uptake experiments twice: once with a bathing solution that produces a negative rest potential, and once with a bathing solution that eliminates the rest potential (Knisley and Grant, 1995; Teruel and Meyer, 1997). Regardless of the value of V_{rest}, the marker molecules were taken up predominately at the hyperpolarized end of the cell. In addition, Part I of this study found that V_{rest} is only important when the electric field is very near the critical value for electroporation. All the experimental studies use much larger fields, so the small offset in potential due to V_{rest} quickly becomes insignificant.

A number of experimental studies have also investigated the effects of the ionic composition and strength of the bathing solution on electroporation and the uptake of marker molecules. Murine myeloma cell in salt solutions (Djuzenova et al., 1996), sea urchin eggs in sea water (Hibino et al., 1991, 1993), and Chinese hamster ovary cells in potassium buffers (Gabriel and Teissie, 1997) were all considered, but the results varied and no clear trend has emerged. One study reported that the ionic strength and composition had no effect (Gabriel and Teissie, 1997), whereas others reported a significant concentration dependence for the location of the marker molecule uptake (hyperpolarized end for low-salt media, depolarized end for high-salt media) (Tekle et al., 1994). With the model of ion-specific electroporation current used here, the ionic concentrations influenced the distribution of N (Fig. 4). Hence, if all ionic concentrations were known, the model could be used to assess whether the experimentally observed differences in molecular uptake with various bathing solutions are due to changes in the current–voltage relationship and N.

Finally, there is at least one study in the literature that reports results that cannot be explained by the ion-specific model. Kinosita and coworkers (Hibino et al., 1991, 1993) observed a complex time course for Ca^{2+} uptake at the poles of the cell, but the overall influx was greater at the depolarized end. These results contradict the predictions of the model with ion-specific electroporation current (Fig. 4 *C*). The difference may be due to the ionic composition of the intracellular and extracellular space or to the intracellular buffering of calcium, but it is also possible that more complex methods of transport such as pressure, osmosis, or streaming are involved. These modes of transmembrane transport are not presently described by the ion-specific model of electroporation, but incorporating one or more of these mechanisms is a possible direction for future development.

COMMENTS

This study presents an extension of the previously developed model of an electroporating single cell (DeBruin and Krassowska, 1999). The ion-specific electroporation current tracks the contribution of individual ion species to the total electroporation current and predicts that an electroporated single cell will have a transmembrane potential profile that is symmetric about the equator and a pore density distribution that is larger at the hyperpolarized end of the cell. The choice of ion species and ionic concentrations in this study was based on information for guinea pig ventricular cells (Luo and Rudy, 1994). For different ion species and/or different ionic concentrations, the pore density profile will change. Hence, the specific results of this study apply only to cells with similar ionic compositions.

The large changes in intracellular ionic concentrations predicted by the model (Fig. 4) may overestimate the local concentration variations in a biological cell. This study assumed that the extracellular ionic concentrations were constant, but a build-up or depletion of ions in a thin layer outside the membrane would limit the movement of ions across the membrane and decrease the variation in intracellular concentrations. In addition, the model of ion-specific electroporation current does not include buffering, sequestering, salt formation, chemical reactions, or any other mechanism that may decrease the number of free ions in solution. However, many of these processes proceed on time scales significantly slower than the 1-ms shock dura-

tion, so the changes in ionic concentrations may be at least transiently large. Simulations of longer shocks or postshock events will require more detailed modeling of the intracellular processes responsible for diffusion and electrical drift of ions.

This study does not investigate electroporation on longer time scales because the membrane model used here has no mechanism by which to extrude specific ions back out of the cell. The best solution to this limitation would be to add ion pumps and exchangers, but such an extension is precarious and unlikely to yield meaningful results without a complete, carefully constructed model of membrane dynamics. Such ionic models do exist, particularly for cardiac cells (DiFrancesco and Noble, 1985; Luo and Rudy, 1994), and they can be combined with the non-specific current (DeBruin and Krassowska, 1998). However, these kinetic models cannot be combined with the ion-specific electroporation current because they treat a cell as a unit and the intracellular ionic concentrations are computed uniformly throughout the entire cell. Both experiments (Knisley and Grant, 1995; Rossignol et al., 1983; Teruel and Meyer, 1997) and the modeling results presented here imply that it is important to track intracellular concentrations locally because of the potentially large influx or efflux of molecules through the pores and the comparatively slow time scale of diffusion. Therefore, to investigate the effects of electroporation on a long time scale, one must develop a model that includes a fairly detailed representation of the ionic current and tracks the spatial distribution of ions inside the cell, accounting for buffering and other significant intracellular processes. This nontrivial extension of the model developed here would allow a more complete investigation of the electrical behavior of the cell during and after an electroporating shock. With active membrane dynamics, the model should be able to test the hypothesis that electroporation may cause postshock disturbances in the cell's electrical behavior as observed experimentally in cardiac muscle (Jones et al., 1978); (Tung et al., 1995).

APPENDIX: ION-SPECIFIC ELECTROPORATION CURRENT

The expression for the ion-specific electroporation current i_{ep} is a more general version of the expression for the non-specific electroporation current derived in detail by Barnett (1990) from the Nernst–Planck equation. The assumptions made about the number, valence, and concentrations of the ion species were discarded to derive a model of electroporation that allows a realistic representation of the ionic composition of the current flowing through the pores. The derivation of an expression for i_{ep} begins with the Nernst–Planck equation that specifies the current density in the pore due to ion species x,

$$i_x = -z_x F D_x \left(\nabla C_x + \frac{z_x F C_x}{RT} \nabla \Phi \right), \tag{A1}$$

where z_x is the valence, D_x is the diffusion coefficient, and C_x is the concentration of ion species x, F is Faraday's constant, R is the universal gas constant, T is absolute temperature, and Φ is the potential within the pore. Assuming that the flow of current is quasi-static and only in the direction y normal to the pore, i_x is constant and can be determined by integrating the Nernst–Planck equation with respect to y. The total current through the pore is a superposition of the current densities carried by all ion species multiplied by the pore's cross sectional area πr_m^2,

$$\begin{aligned} i_{ep} &= \pi r_m^2 \sum_x i_x \\ &= \pi r_m^2 F \sum_x \frac{z_x \left([x]_i \exp\left(\frac{z_x F[\phi_x(0) - \phi_x(h)]}{RT} \right) - [x]_o \right)}{\int_0^h \frac{\exp\left(\frac{z_x F[\phi_x(y) - \phi_x(h)]}{RT} \right)}{D_x} dy}, \end{aligned} \tag{A2}$$

where r_m is the radius of the pore, h is the thickness of the membrane, ϕ_x is the effective potential, and $[x]_i$ and $[x]_o$ are the intracellular and extracellular concentrations of ion species x. The point $y = 0$ is on the intracellular surface of the membrane, and $y = h$ on the extracellular surface. Apart from a slight change in notation and the conversion of number densities to concentrations, Eq. A2 is the same as Eq. 15 in Barnett's derivation (Barnett, 1990).

To simplify Eq. A2, the following assumptions were made (Barnett, 1990).

1. D_x is not a function of position.
2. The effective potential ϕ_x of ion species x is treated as a sum of two components,

$$\phi_x = \phi_{ext} + \phi_{x,B} \tag{A3}$$

where ϕ_{ext} is due to the electric field across the membrane and $\phi_{x,B}$ is the Born energy of an ion in the pore.

3. The potential ϕ_{ext} is assumed to vary linearly across the membrane, from $\phi_{ext}(0) = \phi_i$ to $\phi_{ext}(h) = \phi_e$,

$$\phi_{ext}(y) = v_m \left(1 - \frac{y}{h} \right), \tag{A4}$$

where v_m is the nondimensional transmembrane potential,

$$v_m \equiv \frac{F}{RT} \{ \phi_{ext}(0) - \phi_{ext}(h) \}. \tag{A5}$$

4. The Born energy $\phi_{x,B} \equiv z_x e f(y)$ assumes that the interactions of the ion species x with the walls of the pore are described by a trapezoidal energy barrier $w(y)$ (Glaser et al., 1988),

$$\begin{aligned} w(y) &\equiv \frac{Fe}{RT} \{ f(y) - f(h) \} \\ &= \begin{cases} (y/d) w_o, & 0 \le y \le d \\ w_o, & d \le y \le h - d \\ (h - y/d) w_o, & h - d \le y \le h, \end{cases} \end{aligned} \tag{A6}$$

where e is the charge of an electron and d is the length of the pore entrance.

Using these assumptions, the integral appearing in the denominator of Eq. A2 can be evaluated as

$$\begin{aligned} &\frac{h}{z_x D_x v_m} \left(\frac{w_o z_x \exp[z_x(w_o z_x - n v_m)] - n v_m}{w_o z_x - n v_m} \exp(z_x v_m) \right. \\ &\left. - \frac{w_o z_x \exp[z_x(w_o z_x + n v_m)] + n v_m}{w_o z_x + n v_m} \right), \end{aligned} \tag{A7}$$

where $n \equiv d/h$ is the relative entrance length of the pore. Substituting this expression into Eq. A2 yields the formula for the ion-specific current though a single pore i_{ep}, reported as Eq. 4 in Methods.

This work was supported by the National Institutes of Health Grant HL54071, National Science Foundation Engineering Research Center Grant CDR-8622201, and by a Graduate Fellowship from The Whitaker Foundation.

REFERENCES

Barnett, A. 1990. The current–voltage relation of an aqueous pore in a lipid bilayer membrane. *Biochim. Biophys. Acta.* 1025:10–14.

Chambers, E. L., and J. de Armendi. 1979. Membrane potential, action potential and activation potential of eggs of the sea urchin, *Lytechinus variegatus*. *Exp. Cell. Res.* 122:203–218.

Chang, D. C., B. M. Chassy, J. A. Saunders, and A. E. Sowers, editors. 1992. Guide to Electroporation and Electrofusion. Academic Press, Inc., New York.

DeBruin, K. A., and W. Krassowska. 1998. Electroporation and shock-induced transmembrane potential in a cardiac fiber during defibrillation strength shocks. *Ann. Biomed. Eng.* 26:584–596.

DeBruin, K. A., and W. Krassowska. 1999. Modeling electroporation in a single cell. I. Effects of field strength and rest potential. *Biophys. J.* 77:000–000.

DiFrancesco, D., and D. Noble. 1985. A model of cardiac electrical activity incorporating ionic pumps and concentration changes. *Phil. Trans. R. Soc.* B307:353–398.

Djuzenova, C. S., U. Zimmermann, H. Frank, V. L. Sukhorukov, E. Richter, and G. Fuhr. 1996. Effect of medium conductivity and composition on the uptake of propidium iodide into electropermeabilized myeloma cells. *Biochim. Biophys. Acta.* 1284:143–152.

Gabriel, B., and J. Teissie. 1997. Direct observation in the millisecond time range of fluorescent molecule asymmetrical interaction with the electropermeabilized cell membrane. *Biophys. J.* 73:2630–2637.

Genco, I., A. Gliozzi, A. Relini, M. Robello, and E. Scalas. 1993. Electroporation in symmetric and asymmetric membranes. *Biochim. Biophys. Acta.* 1149:10–18.

Glaser, R. W., S. L. Leikin, L. V. Chernomordik, V F. Pastushenko, and A. I. Sokirko. 1988. Reversible electrical breakdown of lipid bilayers: formation and evolution of pores. *Biochim. Biophys. Acta.* 940:275–287.

Hibino, M., M. Shigemori, H. Itoh, K. Nagayama, and K. Kinosita. 1991. Membrane conductance of an electroporated cell analyzed by submicrosecond imaging of transmembrane potential. *Biophys. J.* 59:209–220.

Hibino, M., H. Itoh, and K. Kinosita. 1993. Time courses of cell electroporation as revealed by submicrosecond imaging of transmembrane potential. *Biophys. J.* 64:1789–1800.

Hille, B. 1992. Ionic Channels of Excitable Membranes. Sinauer Associates Inc., Sunderland, MS. 264.

Jan, L. Y., and Y. N. Jan. 1976. L-glutamate as an excitatory transmitter at the *Drosophilia* larval neuromuscular junction. *J. Physiol.* 262:215–236.

Jones, J. L., E. Lepeschkin, R. E. Jones, and S. Rush. 1978. Response of cultured myocardial cells to countershock-type electric field stimulation. *Am. J. Physiol.* 235:H214–H222.

Kinosita, K., I. Ashikawa, N. Saita, H. Yoshimura, H. Itoh, K. Nagayama, and A. Ikegami. 1988. Electroporation of cell membrane visualized under a pulsed-laser fluorescence microscope. *Biophys. J.* 53: 1015–1019.

Kinosita, K., H. Itoh, S. Ishiwata, K. Hirano, T. Nishizaka, and T. Hayakawa. 1991. Dual-view microscopy with a single camera: real-time imaging of molecular orientations and calcium. *J. Cell Biol.* 115:67–73.

Kinosita, K., M. Hibino, H. Itoh, M. Shigemori, K. Hirano, Y. Kirino, and T. Hayakawa. 1992. Events of membrane electroporation visualized on a time scale from microseconds to seconds. *In* Guide to Electroporation and Electrofusion. D. C. Chang, B. M. Chassy, J. A. Saunders, and A. E. Sowers, editors. Academic Press, Inc., New York. 29–46.

Knisley, S. B., and A. O. Grant. 1995. Asymmetrical electrically induced injury of rabbit ventricular myocytes. *J. Mol. Cell. Cardiol.* 27: 1111–1122.

Krassowska, W. 1995. Effects of electroporation on transmembrane potential induced by defibrillation shocks. *PACE.* 18:1644–1660.

Luo, C.-H., and Y. Rudy. 1994. A dynamic model of the cardiac ventricular action potential. I. Simulations of ionic currents and concentration changes. *Circ. Res.* 74:1071–1096.

Mehrle, W., U. Zimmermann, and R. Hampp. 1985. Evidence for asymmetrical uptake of fluorescent dyes through electro-permeabilized membranes of *Avena* mesophyll protoplasts. *Fed. Eur. Biochem. Soc.* 185: 89–94.

Mehrle, W., R. Hampp, and U. Zimmermann. 1989. Electric pulse induced membrane permeabilisation. Spatial orientation and kinetics of solute efflux in freely suspended and dielectrophoretically aligned plant mesophyll protoplasts. *Biochim. Biophys. Acta.* 978:267–275.

Neu, J. C., and W. Krassowska. 1999. Asymptotic model of electroporation. *Phys. Rev. E.* 59:3471–3482.

Neumann, E., A. E. Sowers, and C. A. Jordan, editors. 1989. Electroporation and Electrofusion in Cell Biology. Plenum Press, New York.

Neunlist, M., and L. Tung. 1997. Dose-dependent reduction of cardiac transmembrane potential by high-intensity electrical shocks. *Am. J. Physiol.* 273:H2817–H2825.

Plonsey, R., and R. C. Barr. 1988. Bioelectricity. A Quantitative Approach. Plenum Press, New York. 50.

River, L. P., R. C. Lee, and F.-S. Pan. 1991. Evidence for electroporation mediated cellular injury in vivo. *Proc. 13th Annual Conf. of the IEEE Engineering in Medicine and Biology Society.* Institute of Electrical and Electronics Engineers, Inc., Piscataway, NJ. 1008–1009.

Rossignol, D. P., G. L. Decker, W. J. Lennarz, T. Y. Tsong, and J. Teissie. 1983. Induction of calcium-dependent, localized cortical granule breakdown in sea-urchin eggs by voltage pulsation. *Biochim. Biophys. Acta.* 763:346–355.

Sowers, A. E. 1988. Fusion events and nonfusion contents mixing events induced in erythrocyte ghosts by an electric pulse. *Biophys. J.* 54: 619–626.

Tekle, E., R. D. Astumian, and P. B. Chock. 1990. Electro-permeabilization of cell membranes: effect of the resting membrane potential. *Biochem. Biophysi. Res. Comm.* 172:282–287.

Tekle, E., R. D. Astumian, and P. B. Chock. 1994. Selective and asymmetric molecular transport across electroporated cell membranes. *Proc. Natl. Acad. Sci. USA.* 91:11512–11516.

Teruel, M. N., and T. Meyer. 1997. Electroporation-induced formation of individual calcium entry sites in the cell body and processes of adherent cells. *Biophys. J.* 73:1785–1796.

Tsong, T. Y. 1991. Electroporation of cell membranes. *Biophys. J.* 60: 297–306.

Tung, L., O. Tovar, M. Neunlist, S. K. Jain, and R. J. O'Neill. 1995. Effects of strong electrical shocks on cardiac muscle tissue. *Ann. NY Acad. Sci.* 720:160–175.

Zhang, L., L. Li, G. A. Hofmann, and R. M. Hoffmann. 1996. Depth-targeted efficient gene delivery and expression in the skin by pulsed electric fields: an approach to gene therapy of skin aging and other diseases. *Biochem. Biophysi. Res. Comm.* 220:633–636.